Journal of Molecular Catalysis A: Chemical 291 (2008) 5–11

Contents lists available at ScienceDirect

Journal of Molecular Catalysis A: Chemical

journal homepage: www.elsevier.com/locate/molcata

Synthesis and photoactivity of Pd substituted nano-TiO_2

R. Vinu, Giridhar Madras*

Department of Chemical Engineering, Indian Institute of Science, Bangalore 560012, India

ARTICLE INFO

Article history:
Received 26 March 2008
Received in revised form 10 July 2008
Accepted 12 July 2008
Available online 23 July 2008

Keywords:
Pd substituted TiO_2
Pd impregnated TiO_2
Photocatalytic degradation
Solution combustion
Dye degradation

ABSTRACT

Palladium substituted and palladium impregnated nanocrystalline anatase titania were prepared by solution combustion method. These catalysts were characterized by XRD, XPS, FT-IR, TGA, BET, UV–vis absorption, TEM and photoluminescence (PL) measurements. The catalysts have been used for the first time for liquid phase photocatalysis. The photocatalytic degradation of various dyes such as Alizarin Red S, Methylene Blue, Orange G and Rhodamine B and phenol and 4-chlorophenol was investigated under UV exposure. Though Pd-ion substituted titania has significantly higher photocatalytic activity compared to unsubstituted titania for NO reduction and NO decomposition, the initial rate of degradation for all the dyes, phenol and 4-chlorophenol was lesser in Pd substituted and impregnated titania compared to that of unsubstituted titania. This reduced reaction rate was attributed to a decrease in the surface area and PL intensity. This study shows that the photoluminescence is the key factor in determining the photocatalytic activity in liquid phase reactions.

1. Introduction

Semiconductor photocatalysis is an emerging area for the effective detoxification of noxious organic water pollutants [1–3]. Photocatalytic degradation results in the demineralization of organic matter into carbon dioxide, water and mineral acids. Although many photocatalysts have been investigated [4] in the past, anatase phase TiO_2 remains the photocatalyst of choice, due to its high photoactivity, low cost and easy synthesis.

Previous studies [5,6] indicate that titania synthesized by solution combustion technique shows superior photocatalytic activity compared to the commercial Degussa P-25 (DP-25) titania. The effect of doping various transition metal ions such as Cu^{2+}, Fe^{3+}, Ce^{4+}, Zr^{4+}, V^{5+} and W^{6+} into combustion synthesized titania has been examined [6]. Though the metal ion doped titania showed an increased photocatalytic activity than the commercial DP-25 TiO_2 catalyst, the catalytic activity was lower than that of the unsubstituted TiO_2. According to the proposed mechanism, the recombination of photogenerated electrons and holes [1,4] is inhibited as the metal scavenges the electrons. This also aids in the generation of hydroxyl radical (•OH), capable of oxidizing organic matter. Other than metal ion substitution, metal ions can also be impregnated on the titania matrix. Metals can also participate with the titania photocatalyst by simply being present on the surface of the TiO_2 matrix, thereby preventing the charge-carrier recombination. While some studies report that the metal ion substituted/impregnated catalysts enhance the photocatalytic degradation rate [7–12], others report a reduction in rate [5,6], thus indicating an optimal metal concentration for high activity. Dyes are an important class of organic water pollutants and, therefore, many studies have been conducted on the photodegradation of dyes and other organic pollutants like phenols, substituted phenols and their mixtures [13–16].

Solution combustion technique has been extensively used for the synthesis of nano-titania [5,6,17] and ZnO nanopowders [18]. Recently, we have shown that Pd-ion substituted titania ($Ti_{0.99}Pd_{0.01}O_{2-\delta}$) has significantly higher photocatalytic activity compared to unsubstituted titania for NO reduction and NO decomposition [19]. In this work, we have explored the liquid phase catalytic properties of this catalyst by examining the degradation of anthraquinonic (Alizarin Red S), heteropolyaromatic (Methylene Blue), xanthene (Rhodamine B) and azoic (Orange G) dyes, and organic pollutants such as phenol and 4-chlorophenol.

2. Experimental

2.1. Catalyst preparation

Nanosize anatase titania was prepared by the solution combustion synthesis methodology. This method involves the combustion of aqueous solutions containing stoichiometric amounts of precursor compound, titanyl nitrate ($TiO(NO_3)_2$) and fuel, glycine ($H_2N–CH_2–COOH$). Titanyl nitrate was synthesized by the reaction of titanyl hydroxide [$TiO(OH)_2$] obtained by the controlled

* Corresponding author. Tel.: +91 80 2293 2321; fax: +91 80 2360 0683.
E-mail address: giridhar@chemeng.iisc.ernet.in (G. Madras).

1381-1169/$ – see front matter © 2008 Elsevier B.V. All rights reserved.
doi:10.1016/j.molcata.2008.07.005

hydrolysis of titanium isopropoxide [Ti(*i*-OPr)$_4$] with nitric acid. The details of the synthesis are reported elsewhere [5]. The combustion mixture for the preparation of 1 at.% Pd/TiO_2 contained titanyl nitrate, palladium chloride ($PdCl_2$) and glycine in the molar ratio 0.99:0.01:1.14. 1 at.% Pd impregnated TiO_2 was prepared by adding calculated amount of $PdCl_2$ drop wise to an aqueous suspension (100 mL) of combustion synthesized TiO_2 in presence of reducing agent, hydrazine hydrate, under magnetic stirring at room temperature. The suspension was stirred for 30 min. The sample was washed with distilled water till all the chloride ions were completely removed and dried at 120 °C for 24 h.

2.2. Catalyst characterization

The catalysts Pd substituted TiO_2 (Pd/TiO_2(sub)), Pd impregnated TiO_2 (Pd/TiO_2(imp)), unsubstituted combustion synthesized TiO_2 (CS TiO_2) and commercial DP-25 TiO_2 were characterized by various techniques. The X-ray diffraction (XRD) patterns were recorded on a Philips X'pert Pro Diffractometer with Cu Kα radiation in the 2θ range from 20° to 80° at a scanning rate of 1°/min. The X-ray photoelectron spectra (XPS) were recorded with ESCA-3 Mark II spectrometer (VG Scientific Ltd., UK) using Al Kα radiation (1486.6 eV). Fourier transform-infra red (FT-IR) studies were carried out with Perkin-Elmer (FT-IR-Spectrum-1000) spectrometer in the transmission mode. Thermo-gravimetric analysis (TGA) was carried out with a thermal analyzer (Perkin-Elmer, Pyris Diamond) to determine the adsorbed water. UV–vis absorption spectra were obtained using Perkin-Elmer UV–visible spectrophotometer. Every sample was dry pressed into a 10 mm diameter round disk containing about 150 mg of catalyst. Absorption spectra were referenced to $BaSO_4$. Transmission electron microscopy (TEM) of 1 at.% Pd/TiO_2(sub) and 1 at.% Pd/TiO_2(imp) was carried out using JEOL JEM-200CX operated at 200 kV. The photoluminescence (PL) measurements were performed in a luminescence spectrophotometer (Perkin-Elmer 55) operated at room temperature.

2.3. Photoreactor

The photocatalytic activity of 1 at.% Pd/TiO_2(sub) and 1 at.% Pd/TiO_2(imp) was evaluated by measuring the degradation rates under UV exposure. The activity of the catalyst was compared with CS TiO_2 and DP-25 TiO_2. The photochemical reactor employed in the present study consisted of a jacketed quartz tube of 3.4 cm i.d., 4 cm o.d., and 21 cm length. A high-pressure mercury vapor lamp of 125 W (Philips, India) that radiated predominantly at 365 nm (3.4 eV) was placed inside the reactor after carefully removing the outer shell. Water was circulated through the annulus to avoid heating during the reaction. Further details are provided elsewhere [5].

The catalyst concentration employed in the current study was 1 g L^{-1} for all the catalysts and all the experiments were performed in the natural pH of the dye. The initial concentration employed for the dye solutions range from 10 mg L^{-1} to 100 mg L^{-1}.

2.4. Sample analysis

Before analyzing the degraded samples of all the dyes and phenols, the samples were filtered using Millipore membrane filters and centrifuged to remove the catalyst particles prior to analysis. For the analysis of dyes, the centrifuged sample was used to record the UV–vis spectra (Systronics, Spectrophotometer-166) in the wavelength range 200–800 nm. The characteristic wavelength, λ_{max} values are 420 nm, 664 nm, 475 nm and 553.6 nm for Alizarin Red S (ARS), Methylene Blue (MB), Orange G (OG) and Rhodamine B (RB), respectively. For all the dyes, calibration based on Beer–Lambert law was used to quantify the concentration.

Several intermediates are formed during the degradation of phenols [14,15]. To quantify these intermediates, the samples were analyzed in HPLC. The HPLC consisted of an isocratic pump (Waters 501), Rheodyne injector (model 7010, sample loop-50 μL), C-18 column, UV detector (Waters 2487) and a data acquisition system. The eluent stream consisted of 90:10 (v/v) water:methanol pumped at 0.5 mL/min for analyzing phenol and 4-chlorophenol. The UV absorbance detector was set at 270 nm and 280 nm for phenol and 4-chlorophenol, respectively. The chromatographic areas were converted to concentration values using the calibration curves based on pure compounds. The compounds were identified and the concentrations were further verified by LC–MS (Waters 3100 Mass Detector).

Many of the experiments were repeated in triplicate and the error in the determination of the concentration was ±1 mg L^{-1}. Experiments were conducted in aqueous solutions with pH varying from 2 to 11. The XRD pattern before and after the experiment showed no change indicating that the material is stable and no metal was leaching out from the catalyst into solution.

3. Results and discussion

3.1. Catalyst characterization

The XRD patterns of 1 at.% Pd/TiO_2(sub) and 1 at.% Pd/TiO_2(imp) are shown in Fig. SI 1 (see supplementary data). The pattern can be indexed to TiO_2 in the anatase phase only. The rutile and brookite phases were not observed. The crystallite size is determined from the (1 0 1) peak in the XRD pattern using the Scherrer formula, and the average size of both Pd substituted and impregnated titania crystallites were 8–10 nm. Rietveld refinements of the diffraction patterns of $Ti_{0.99}Pd_{0.01}O_{2-\delta}$, 1 at.% Pd/$TiO_2$(imp) were carried out using the FullProf-98 program, and a good agreement between calculated and observed pattern was obtained. The flat background indicates that the Pd substituted titania is crystalline in nature. The change in lattice parameters, R_{bragg} and R_f with respect to combustion synthesized TiO_2 are listed in Table S1 (see supplementary data).

Pd metal peaks (1 1 1) were not found in the XRD patterns of 1% Pd/TiO_2(sub). However, for 3% Pd/TiO_2, rutile phase goes up to 30% and Pd (1 1 1) peaks appear [19]. The diffraction lines due to PdO were also not present in 1% Pd/TiO_2(sub). However, 1% Pd/TiO_2(imp) indeed shows Pd (1 1 1) peaks. The absence of Pd (1 1 1) peak and diffraction lines due to PdO in the combustion synthesized sample of 1% Pd/TiO_2 suggests the formation of $Ti_{0.99}Pd_{0.01}O_{1.99}$. Further, the Rietveld refinement of 1% Pd/TiO_2(sub) has been carried out and the difference plot does not show detectable peaks due to Pd or PdO [19].

The Pd($3d_{5/2,3/2}$) core level spectra of Pd metal powder, 1% Pd/TiO_2(imp), PdO and 1% Pd/TiO_2(sub) are presented in Fig. SI 2. Pd($3d_{5/2,3/2}$) peaks at 335 eV and 340.5 eV indicate that Pd metal is in zero valent state. In the Pd impregnated TiO_2 also, binding energy of Pd($3d_{5/2,3/2}$) peaks are at 335 eV and 340.5 eV. Pd($3d_{5/2,3/2}$) peaks at 336.8 eV and 342.2 eV in the PdO sample shows that Pd is in 2+ state. In the combustion synthesized Pd/TiO_2(sub), Pd($3d_{5/2}$) core level binding energy is at 337.2 eV. Thus the binding energy of Pd ions in TiO_2 is higher than Pd^{2+} in PdO. Thus, Pd in the combustion synthesized TiO_2 is in 2+ state and PdO diffraction lines are absent in the XRD. Further, based on XPS data and the peak intensities [19], the surface concentration of Pd^{2+} ion in 1 at.% Pd/TiO_2(sub) is 2.3% as against 9.4% in the Pd metal impregnated on TiO_2. Thus, Pd ion is indeed substituted in TiO_2 crystallites.

The FT-IR spectrum of Pd/TiO_2(sub) was compared with that of CS TiO_2 and DP-25 TiO_2 (Fig. SI 3). The broad, strong peaks at 3340 cm^{-1} and 1625 cm^{-1} show the characteristic absorption of δ(–OH) stretching and bending mode of δ(–O–H) functional group, which is due to Ti–OH and hydrated species. There is a noticeable difference between CS TiO_2 and Pd/TiO_2(sub) with area reduction for the very large band at 3400 cm^{-1} and for the 1640 cm^{-1} in case of Pd/TiO_2(sub) compared to that of CS TiO_2.

The TEM image of 1 at.% Pd/TiO_2(sub) is shown in Fig. SI 4(a). The particle size range is 8–10 nm. Fig. SI 4(b) shows the ring type diffraction pattern of 1 at.% Pd/TiO_2(sub) and 1 at.% Pd/TiO_2(imp), where the presence and absence of the diffraction lines of Pd metal are clearly elucidated in 1 at.% Pd/TiO_2(imp) and 1 at.% Pd/TiO_2(sub), respectively.

Thus, based on XRD, XPS and TEM, one can conclude that Pd^{2+} ions are substituted in the TiO_2 matrix and 1% Pd/TiO_2(sub) can be represented as $Ti_{0.99}Pd_{0.01}O_{1.99}$. Because Pd is in 2+ state in the Ti site, there has to be at least one oxide ion vacancy for Pd^{2+} ion to satisfy charge balance.

Fig. 1a shows the TGA plot of CS TiO_2, 1 at.% Pd/TiO_2(sub), 1 at.% Pd/TiO_2(imp) and DP-25 TiO_2 employed in the present study. The analysis was carried out in an inert nitrogen atmosphere with a flow rate of 150 cm^3 min^{-1} and a heating rate of 5 °C min^{-1}. Three regions of weight loss in the TGA curve are observed. The first stage up to 150 °C corresponds to the loss of physically adsorbed water; the second stage from 150 °C to 500 °C is due to the removal of strongly bound water or surface hydroxyl groups from the catalyst. In the third stage from 500 °C to 800 °C, the weight loss is less than 0.5%. The weight loss among the four catalysts is in the following order: Pd/TiO_2(sub) ≈ CS TiO_2 > Pd/TiO_2(imp) > DP-25 TiO_2. Among the four catalysts, Pd/TiO_2(sub) shows a maximum total weight loss of 16.2%, while Degussa P-25 shows the least weight loss of 1.4%. A weight loss of 10.4% and 15.6% is observed for Pd impregnated and unsubstituted TiO_2, respectively. Thus the amount of adsorbed water or surface hydroxyl groups is comparable in Pd/TiO_2(sub) and CS TiO_2.

The UV–vis absorption spectra of all the four catalysts are shown in Fig. 1b. Pd doping has a significant effect on the absorption characteristics of TiO_2. CS TiO_2 shows two optical absorption thresholds at 570 nm and 467 nm that correspond to band gap energies of 2.18 eV and 2.65 eV, respectively. The Pd substituted and impregnated TiO_2 show absorption bands at 418 nm and 425 nm, which correspond to band gap energies of 2.96 eV and 2.92 eV, respectively, which is still lesser than that of DP-25 of 3.1 eV. The electronic transitions from the valence band to dopant level or from the dopant level to the conduction band can effectively red shift the band edge absorption threshold. Thus optical absorption of metal-doped systems depends on the energy level of the dopants within the TiO_2 lattice, their d electronic configuration, and the distribution of the dopant metal ions [6].

The PL technique has been widely used in the field of photocatalysis over solid semiconductors as a useful probe for understanding the surface processes in which photogenerated electrons and holes take part, i.e., primary processes in photocatalysis. Fig. 1c shows

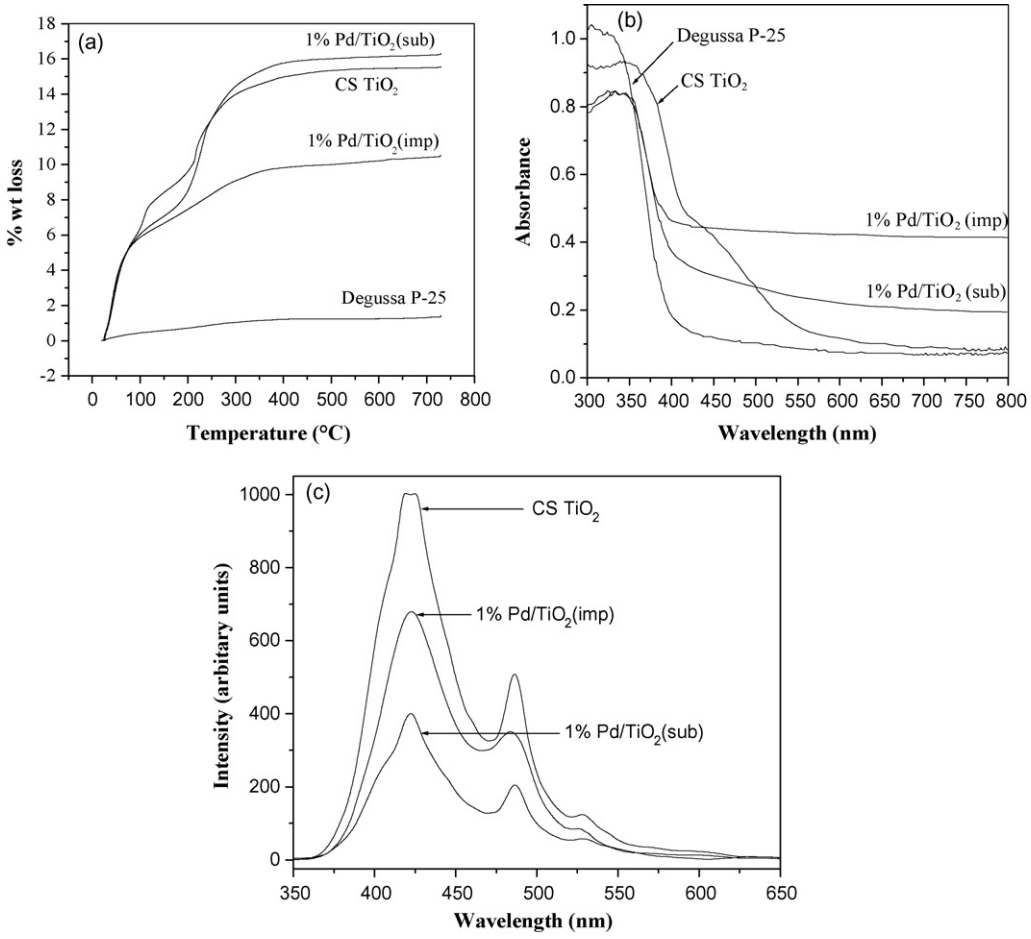

Fig. 1. (a) TGA, (b) UV–vis absorption spectra of CS TiO_2, 1 at.% Pd/TiO_2(sub), 1 at.% Pd/TiO_2(imp) and DP-25 and (c) photoluminescence spectra of CS TiO_2, 1 at.% Pd/TiO_2(sub) and 1 at.% Pd/TiO_2(imp).

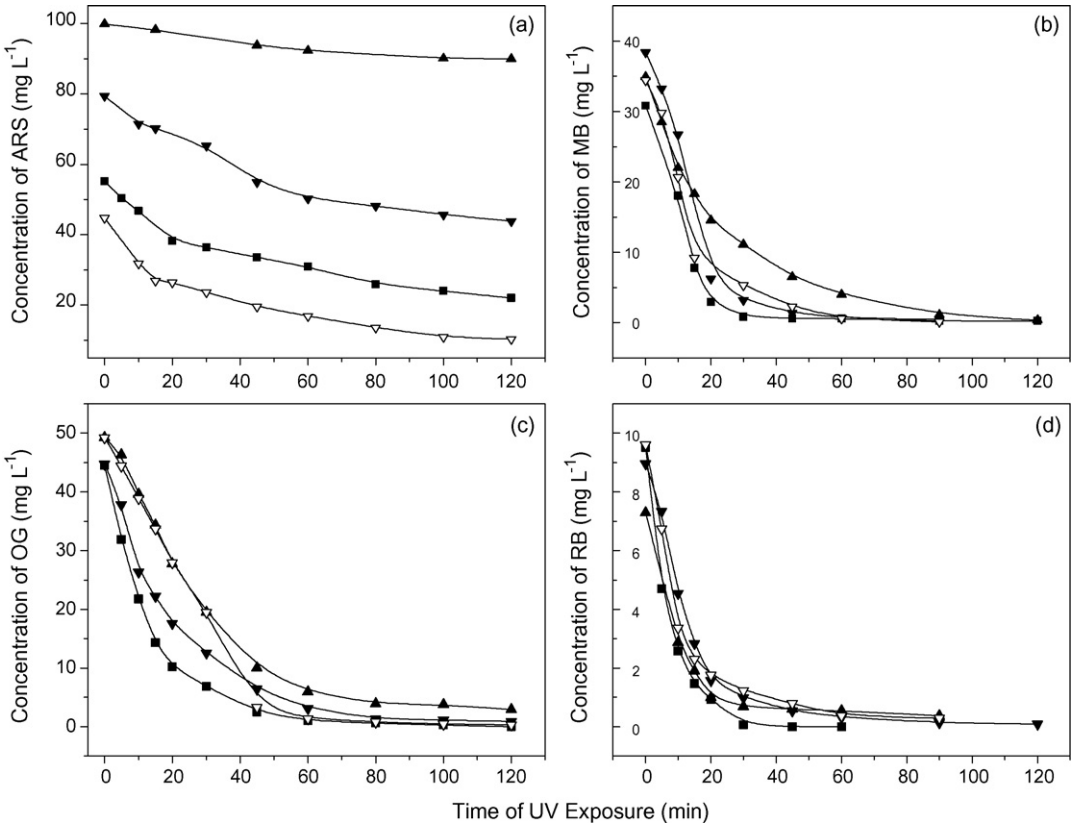

Fig. 2. Concentration profile of (a) ARS, (b) MB, (c) OG and (d) RB [legend for all panels: (■) CS TiO_2, (▲) DP-25, (▼) Pd/TiO_2(sub) and (▽) Pd/TiO_2(imp)].

the PL emission spectra of CS TiO_2, Pd/TiO_2(sub) and Pd/TiO_2(imp). The spectrum of CS TiO_2 exhibits two emission peaks at 419 nm and 483 nm with excitation at 285 nm. The emission band at 419 nm is due to free exciton emission of TiO_2. The emission band at 483 nm is due to the surface state Ti^{4+}–OH. Though Pd/TiO_2(sub) exhibits emission spectrum at the same energy as that of CS TiO_2, the PL intensities are much lower than that of CS TiO_2 indicating that the PL intensities are quite sensitive to doping. The quenching increases with the increase in amount of doping. This is attributed to the enhanced metal–metal interaction at higher concentrations. Since excitation was carried out under the same absorption conditions at 285 nm, a decrease in the emission intensities must originate from the differences in the electronic structure of the metal-doped samples. The observed decrease in the intensity on Pd doping can be attributed to oxide ion vacancy that can trap a photogenerated conduction band electron, which subsequently recombines with a valence band hole. It is interesting to note that Pd/TiO_2(imp) exhibits higher PL intensities corresponding to 419 nm and 483 nm compared to Pd/TiO_2(sub), but significantly lower than that of undoped CS TiO_2. This may be because the impregnation of Pd onto the surface of CS TiO_2 acts as a support, which prevents the recombination of holes and electrons. Thus, the degradation rate of dyes and organics in presence of these catalysts follows the same order as their PL intensity.

The BET surface area for 1 at.% Pd/TiO_2(sub) catalyst was determined by nitrogen adsorption–desorption method at liquid nitrogen temperature using a Quantachrome NOVA 1000 surface area analyzer and the value was 50 m^2/g [19], which is considerably lesser than 156 m^2/g for unsubstituted titania [6]. The surface area of 1 at.% Pd/TiO_2(sub) catalyst was considerably lower than CS TiO_2 due to larger size of the particle. While, 1% Pd substituted TiO_2 had a particle size range between 8 nm and 10 nm, the unsubstituted titania has a particle size range of 4–6 nm.

3.2. Photocatalytic degradation studies

Degradation experiments for all the dyes ARS, MB, OG and RB were carried out with CS TiO_2, 1 at.% Pd/TiO_2(sub), 1 at.% Pd TiO_2(imp) and commercial DP-25 TiO_2 catalysts. No detectable degradation of the dyes was observed without catalyst or irradiation with UV light alone.

The initial concentrations of ARS, MB, OG and RB were 100 mg L^{-1}, 40 mg L^{-1}, 50 mg L^{-1} and 10 mg L^{-1}, respectively. Before degrading the dye solutions with UV light, they were allowed to adsorb on the catalyst surface by stirring the mixture in the dark for 30 min. The adsorbed dye concentration was then used as the initial concentration for subsequent degradation under UV exposure. Fig. 2(a)–(d) shows the degradation rate profile for all the dyes with four catalysts. There is significant adsorption of ARS on CS TiO_2 and Pd/TiO_2(imp). This increased adsorption can be attributed to the higher surface area as compared with the other catalysts. Initial rates were calculated for the degradation of all the dyes with all the catalysts within 5–10 min of UV exposure and it was found that for all the dyes, CS TiO_2 showed a better degradation rate than all the other catalysts and DP-25 exhibited the slowest rate. The initial rates for the degradation of ARS, MB, OG and RB with Pd/TiO_2(sub) and Pd/TiO_2(imp) were 0.80 and 0.92 mg L^{-1} min^{-1}, 1.16 and 1.38 mg L^{-1} min^{-1}, 1.2 and 1.04 mg L^{-1} min^{-1} and 0.44 and 0.62 mg L^{-1} min^{-1}, respectively. This shows that impregnation of Pd onto CS TiO_2 is more beneficial than substitution for the degradation of the dyes.

The concentration profiles of phenol and 4-chlorophenol are shown in Fig. 3(a) and (b). In the case of phenol, for an initial concen-

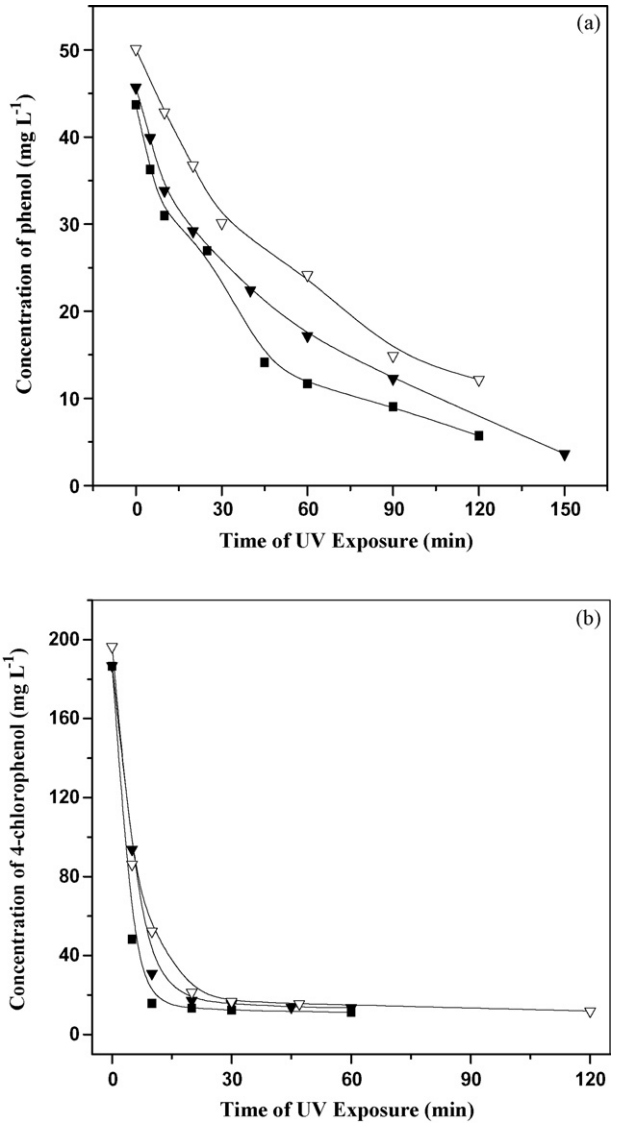

Fig. 3. Concentration profiles of (a) phenol and (b) 4-chlorophenol [legend: (■) CS TiO_2, (▼) Pd/TiO_2(sub) and (▽) Pd/TiO_2(imp)].

tration of 45 mg L^{-1}, the initial rate of photocatalytic degradation was 1.3, 0.96 and 0.73 mg L^{-1} min^{-1} for CS TiO_2, Pd/TiO_2(sub) and Pd/TiO_2(imp), respectively. In the case of 4-chlorophenol, for an initial concentration of 187 mg L^{-1}, the initial rate of photocatalytic degradation was 28, 22 and 18 mg L^{-1} min^{-1} for CS TiO_2, Pd/TiO_2(imp) and Pd/TiO_2(sub), respectively. The results show that CS TiO_2 exhibits a higher rate of photocatalytic degradation for both phenol and 4-chlorophenol, compared to the other two catalysts. Among Pd/TiO_2(sub) and Pd/TiO_2(imp), the latter exhibits a better initial rate of degradation of 4-chlorophenol compared to Pd/TiO_2(sub), while the initial rate of degradation of phenol is comparable with both the catalysts. Thus, the above results are consistent with the trend observed for the degradation of dyes, which can be correlated with the high PL intensity for Pd/TiO_2(imp) compared to Pd/TiO_2(sub).

No reaction intermediates were observed when phenol was degraded with an initial concentration of 45 mg L^{-1} in presence of all the catalysts except for DP-25 TiO_2 (Fig. 4). This is because the amount of intermediates formed could be below our detection limit of 1 mg L^{-1}. However, when we increased the initial concentration of phenol to 200 mg L^{-1}, around 10 mg L^{-1} of the intermediates

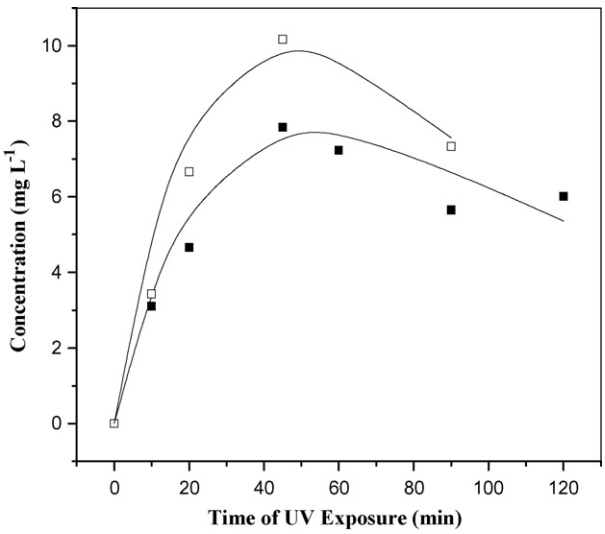

Fig. 4. Concentration profile of hydroquinone and catechol obtained during the degradation of phenol with DP-25 [legend: (□) hydroquinone and (■) catechol; lines: model fit].

were observed but they quickly disappeared. This is because of the high rates of secondary hydroxylation compared to that of the primary hydroxylation. In the case of degradation of 4-chlorophenol in presence of CS TiO_2, an initial concentration of 50 mg L^{-1} results in no observable intermediates, consistent with our previous study [14]. However, when the initial concentration was chosen to be 187 mg L^{-1}, the intermediates could be clearly observed, as shown in Fig. 5.

Direct holes and hydroxyl radicals are responsible for the degradation of organic compounds. The holes generated due to the excitation of electrons combine with the surface hydroxyl species on TiO_2 to form the hydroxyl radical. These radicals degrade the organics. The degradation of phenols proceeds through a stepwise formation of the intermediates. The primary hydroxylation of the organics results in intermediates like hydroquinone and catechol. These aromatic intermediates undergo further secondary hydroxylation and ring cleavage to yield carboxylic acids and aldehydes. In this study, the above two primary intermediates alone were detected, when analyzed by HPLC. These intermediates undergo secondary hydroxylation and then, ring opening reaction and forms aliphatic intermediates, which further degrade giving rise to CO_2 and water vapor. The concentration of all the intermediates increases initially and then exhibits a decrease in trend. The maximum in the concentration of the intermediates is observed due to the competition between the primary hydroxylation and the secondary hydroxylation step. The degradation pathway for the pollutants can be described when the initial pollutant degrades to primary hydroxylated intermediates, which further degrades to secondary hydroxylated intermediates and ring opened fragments [14]. Assuming all the reactions to be first order, for a series reaction, the concentration of the intermediate is given by, $C_{int}/C_{A0} = k_f/k_c - k_f(\exp(-k_f t) - \exp(-k_c t)$, where C_{int} is the concentration of the intermediate at any time t, C_{A0} is the initial concentration of the pollutant A, k_f and k_c denote the formation and consumption rate constant of the intermediate, respectively. The maximum concentration of the intermediate, $C_{int,max}$, and the corresponding time, t_{max} can be obtained from the above equation and are given by [14]:

$$\frac{C_{int,max}}{C_{A0}} = \left(\frac{k_f}{k_c}\right)^{1/((1-k_f)/k_c))} \quad (1)$$

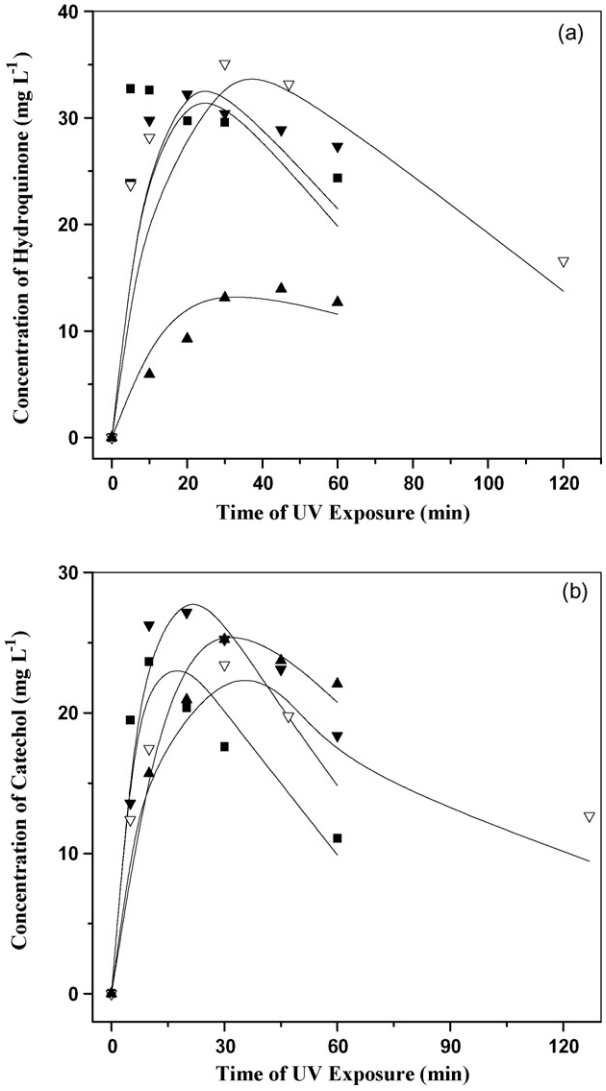

Fig. 5. Concentration profiles of (a) hydroquinone and (b) catechol obtained during degradation of 4-chlorophenol [legend: (■) CS TiO_2, (▲) DP-25, (▼) Pd/TiO_2(sub) and (▽) Pd/TiO_2(imp); lines: model fit].

$$t_{max} = \frac{\ln(k_f/k_c)}{k_c((k_f/k_c) - 1)} \quad (2)$$

The concentration profile of the intermediates obtained experimentally is fitted with Eqs. (1) and (2) to determine k_f and k_c for hydroquinone and catechol. Figs. 4 and 5 show the concentration profile of the intermediates for phenol in presence of DP-25 TiO_2 and 4-chlorophenol in presence of all the catalysts, respectively. The values of k_f and k_c for the primary hydroxylated intermediates are listed in Table 1. The ratio k_c/k_f for 4-chlorophenol is almost similar for CS TiO_2, Pd/TiO_2(sub) and Pd/TiO_2(imp). In all the cases, the value of k_c is higher than that of k_f, indicating that the secondary hydroxylation and subsequent reaction steps are faster than the primary hydroxylation step and thus no detectable amount of secondary hydroxylated species was observed. This is attributed to the fact that hydroxylated organics undergo faster oxidation than non-hydroxylated organics. Due to the presence of more surface hydroxyl groups in combustion synthesized catalyst, the rate of secondary hydroxylation is significantly higher than the rate of primary hydroxylation. Our future studies will involve determination of the catalytic activity of other metal ion substituted catalysts and explore methods to immobilize these catalysts using techniques reported in the literature [20,21].

Table 1
The formation and consumption rate constants of the intermediates formed by the degradation of phenol in presence of DP-25 TiO_2 and 4-chlorophenol in presence of CS TiO_2, 1 at.% Pd/TiO_2(sub), 1 at.% Pd/TiO_2(imp) and DP-25 TiO_2

Pollutant	Catalyst	Intermediates	k_c (min^{-1})	k_f (min^{-1})	k_c/k_f
Phenol	DP-25 TiO_2	Hydroquinone	0.036	0.013	2.67
		Catechol	0.036	0.009	3.91
4-Chlorophenol	CS TiO_2	Hydroquinone	0.070	0.021	3.32
		Catechol	0.130	0.025	5.20
	1% Pd/TiO_2(sub)	Hydroquinone	0.075	0.021	3.51
		Catechol	0.095	0.023	4.13
	1% Pd/TiO_2(imp)	Hydroquinone	0.050	0.015	3.33
		Catechol	0.071	0.012	5.82
	DP-25 TiO_2	Hydroquinone	0.07	0.01	7.00
		Catechol	0.051	0.018	2.83

4. Conclusions

Two catalysts, palladium substituted and palladium impregnated nanocrystalline anatase titania, were prepared and used for liquid phase catalysis for the first time. Though $Ti_{0.99}Pd_{0.01}O_{2-\delta}$ had a lower surface area and higher band gap compared to that of unsubstituted titania, it had shown higher photocatalytic activity compared to unsubstituted titania for gas-phase NO reduction [19]. This was attributed due to the adsorption and subsequent dissociation of NO on the oxide ion vacancy. However, for liquid phase catalysis of dyes and phenols, this catalyst shows decreased photocatalytic activity compared to that of unsubstituted titania. The reason for the decreased activity of Pd substituted titania is also supported by the PL spectroscopy. The spectra show that the luminescence intensity of Pd substituted titania is lesser than that of unsubstituted and Pd impregnated titania. This decreased luminescence is due to shunting of the electron density that can trap a photogenerated conduction band electron, which subsequently recombines with a valence band hole. The combination of a reduction of surface area, increase of band gap and decreased PL intensity leads to the lowering of catalytic activity of Pd substituted titania compared to that of unsubstituted titania in case of liquid phase reactions.

Acknowledgment

The corresponding author thanks the department of science and technology for the swarnajayanthi fellowship and Professor M.S. Hegde for very helpful discussions.

Appendix A. Supplementary data

Supplementary data associated with this article can be found, in the online version, at doi:10.1016/j.molcata.2008.07.005.

References

[1] M.R. Hoffmann, S.T. Martin, W. Choi, D.W. Bahnemann, Chem. Rev. 95 (1995) 69.
[2] M.A. Fox, M.T. Dulay, Chem. Rev. 93 (1993) 341.
[3] A. Hagfeldt, M. Grätzel, Chem. Rev. 95 (1995) 49.
[4] D.S. Bhatkhande, V.G. Pangarkar, A.A.C.M. Beenackers, J. Chem. Technol. Biotechnol. 77 (2001) 102.
[5] G. Sivalingam, K. Nagaveni, M.S. Hegde, G. Madras, Appl. Catal. B 45 (2003) 23.
[6] K. Nagaveni, M.S. Hegde, G. Madras, J. Phys. Chem. B 108 (2004) 20204.
[7] C. He, Y. Yu, X. Hu, A. Larbot, Appl. Surf. Sci. 200 (2002) 239.
[8] S.X. Liu, Z.P. Qu, X.W. Han, C.L. Sun, Catal. Today 93 (2004) 877.

[9] B.N. Ohtani, K. Iwai, S. Nishimoto, S. Sato, J. Phys. Chem. B 101 (1997) 3349.
[10] Y.M. Gao, W. Lee, R. Trehan, R. Kershaw, K. Dwight, A. Wold, Mater. Res. Bull. 26 (1991) 1247.
[11] R.J. Tayade, R.G. Kulkarni, R.V. Jasra, Ind. Eng. Chem. Res. 45 (2006) 5231.
[12] C. Chen, X. Li, W. Ma, L. Zhao, H. Hidaka, N. Serpone, J. Phys. Chem. B 106 (2002) 318.
[13] J. D'Oliveira, G. Al-sayyed, P. Pichat, Environ. Sci. Technol. 24 (1990) 990.
[14] G. Sivalingam, M.H. Priya, G. Madras, Appl. Catal. B: Environ. 51 (2004) 67.
[15] W.F. Jardim, S.G. Moraes, M.M.K. Takiyama, Water Res. 31 (1997) 1728.
[16] R.M. Alberici, W.F. Jardim, Water Res. 28 (1994) 1845.
[17] Y. Cheng, H. Sun, W. Jin, N. Xu, Chem. Eng. J. 128 (2007) 127.
[18] S. Park, H.-J. Park, K. Yoo, H.S. Kim, J.C. Lee, Y.-J. Chung, J.-H. Lee, M.K. Park, J. Phys. Chem. Solids 69 (2008) 1495.
[19] S. Roy, M.S. Hegde, N. Ravishankar, G. Madras, J. Phys. Chem. 111 (2007) 8153.
[20] Y. Chen, D.D. Dionysiou, Appl. Catal. A: Gen. 317 (2007) 129.
[21] N. Strataki, V. Bekiari, D.I. Kondarides, P. Lianos, Appl. Catal. B: Environ. 77 (2007) 184.